Loading rates in California inferred from aftershocks

C. Narteau

Laboratoire de Dynamique des Fluides Géologiques, Institut de Physique du Globe de Paris, 75252 Paris Cedex 05, France

P. Shebalin

International Institute of Earthquake Prediction and Mathematical Geophysics, Warshavskoye shosse, 79, korp 2, Moscow 113556, Russia

M. Holschneider

Institutes of Applied and Industrial Mathematics, Universtität Potsdam, POB 601553, 14115 Potsdam, Germany.

C. Narteau, Laboratoire de Dynamique des Fluides Géologiques, Institut de Physique du Globe de Paris, 75252 Paris Cedex 05, France (narteau@ipgp.jussieu.fr)

P. Shebalin, International Institute of Earthquake Prediction Theory and Mathematical Geophysics, Warshavskoye shosse, 79, korp 2, Moscow 113556, Russia. (shebalin@mitp.ru)

M. Holschneider, Institutes of Applied and Industrial Mathematics, Universtität Potsdam, POB 601553, 14115 Potsdam, Germany. (hols@math.uni-potsdam.de)

Abstract.

We estimate the loading rate in southern California and the change in stress induced by a transient slip event across the San Andreas fault (SAF) system in central California, using a model of static fatigue. We analyze temporal properties of aftershocks in order to determine the time delay before the onset of the power law aftershock decay rate. In creep-slip and stick-slip zones, we show that the rate of change of this delay is related to seismic and aseismic deformation across the SAF system. Furthermore, we show that this rate of change is proportional to the deficit of slip rate along the SAF. This new relationship between geodetic and seismological data is in good agreement with the prediction of a Limited Power Law model in which the evolution of the duration of a linear aftershock decay rate over short time results from variations in the load of the brittle upper crust.

1. Introduction

In the last decades, geodetic measurements have improve considerably the description of spatio-temporal properties of strain accumulation and release along faults [*Savage and Burford*, 1973; *Sauber et al.*, 1986; *Langbein et al.*, 1990; *Bennett et al.*, 1996; *Peltzer et al.*, 2001; *Fialko*, 2006]. Overall, these new sets of data may now enable to deliver a range of informations over time scales that approach the characteristic times of loading and discharge along faults. An important result is that, complementary to the deformation accommodated by earthquakes, aseismic deformation such as post-seismic slip [*Langbein*, 1990], slow earthquakes [*Dragert et al.*, 2001] and creep [*Simpson et al.*, 2001], may accommodate an important part of the deformation. Then, a challenge for seismic hazard assessment remains to couple these different modes of deformation with different patterns of seismicity [*Nadeau and Mcevilly*, 1999, 2004; *Schmidt et al.*, 2005; *Schorlemmer et al.*, 2005; *Schorlemmer and Wiemer*, 2005].

Aftershocks are earthquakes of smaller magnitude that occur after an event in the neighborhood of the seismogenic rupture. The aftershock rate decays with time according to a power law [*Omori*, 1894], and, just after the mainshock, this rate is essential in determining physical mechanisms ruling the transition from the dynamic rupture to the relaxation phase [*Kagan and Houston*, 2005]. Unfortunately, it is extremely difficult to evaluate the exact aftershock frequency over short time: identification of aftershocks in coda waves of mainshock, overlapping aftershock records, catalog compilers overload, absence or malfunction of seismic stations close to the source zone. Then, solutions consists in scrutinizing the high-frequency signal [*Vidale et al.*, 2004], or analyzing aftershocks of larger magnitude which are more likely to be observed [*Utsu et al.*, 1995]. In both cases,

non power law behavior could remain at the beginning of the aftershock sequence [*Narteau et al.*, 2002; *Peng et al.*, 2006, 2007; *Enescu et al.*, 2007].

An usual measure of the time delay before the onset of the power law aftershock decay rate is the parameter c of the modified Omori law (MOL),

$$\Lambda(t) = \frac{K}{(c+t)^p}, \tag{1}$$

where K is a constant aftershock rate, t is the elapsed time from the mainshock and p is the slope of the power law aftershock decay rate [*Utsu et al.*, 1995]. In a vast majority of cases, the c-value is determined empirically and its magnitude is only discussed with respect to the artifacts cited above. Inspired by a model of static fatigue suggested by *Scholz* [1968], *Narteau et al.* [2002] proposed a physical interpretation to the parameter c of the MOL by relating its magnitude to an upper limit of the overload within the aftershock zone. *Narteau et al.* [2005] have tested such a prediction in southern California and have shown that, at a regional length scale, the evolution of the c-value exhibits an asymmetry which may be related to the classical seismic cycle picture (i.e. slow loading and rapid discharge).

In the present paper, we study the central segment of the San Andreas fault (SAF) where, instead of large $M > 7$ earthquakes, the seismicity is characterized by small earthquakes along the creeping segment, and $M \approx 6$ earthquakes near Parkfield, along the transition zone between the creeping and locked behavior of the fault. Most of these $M \approx 6$ earthquakes occurs on the SAF, as it was the case in 1857, 1881, 1901, 1922, 1934, 1966 and on the September 28, 2004. Nevertheless, the 1983, $M6.5$ Coalinga earthquake in the west, and the 2003, $M6.5$ San Simeon earthquake in the east indicate that, across the boundary between the American plate and the Pacific plate, the deformation is distributed

on a population of faults and on off-fault structures [*Titus et al.*, 2005]. Hence, we take advantage of the spatial distribution of seismic events and of the systematic occurrence of aftershocks to provide, through a model of static fatigue, an estimation of loading and unloading rates across the SAF system.

2. A band-limited power law model of aftershock decay rate

In order to model the aftershock decay rate, let us describe briefly the relaxation mechanism which is fully exposed in *Narteau et al.* [2002] and generalized to any stress history in *Narteau* [2007].

In the aftershock zone, we consider a finite population of domains which are able to fail under continued static overload. Each failure results of aging accelerated by stress perturbations induced by the mainshock and changes in the strength of the rock. Assuming that each domain can produce a single aftershock, the characteristic time of this event is given by a relationship between the overload σ_0 and failure rate λ. Classical expressions of $\lambda(\sigma_0)$ are based on subcritical crack growth experiments [*Atkinson and Meredith*, 1987] and empirical relationships between the stress intensity factor and the crack velocity. In all cases, the failure rate is an increasing function of the stress perturbation with either an exponential [*Charles and Hillig*, 1962; *Wiederhorn and Bolz*, 1970] or a power-law [*Charles*, 1958; *Atkinson*, 1984] shape. In addition to this rate, $N(\sigma_0, t)$, the overload distribution over the population of domain is enough to evaluate the aftershock rate $\Lambda(t)$ in a probabilistic fashion:

$$\Lambda(t) = \int_0^\infty N(\sigma_o, t)\lambda(\sigma_o)d\sigma_o. \tag{2}$$

For any single overload value, the aftershock rate is

$$\frac{\partial N(\sigma_o, t)}{\partial t} = -\lambda(\sigma_o) N(\sigma_o, t). \tag{3}$$

Injecting the solution of Eq. 3 into Eq. 2 yields

$$\Lambda(t) = \int_0^\infty \mathcal{N}(\sigma_o)\lambda(\sigma_o) \exp\left(-\lambda(\sigma_o)t\right) d\sigma_o. \tag{4}$$

where $\mathcal{N}(\sigma_o) = N(\sigma_o, 0)$ is the overload distribution just after the mainshock. The aftershock decay rate is therefore a sum of exponential decay rates, and *Narteau et al.* [2002] have shown that various failure rates $\lambda(\sigma_0)$ and simplified overload distributions $\mathcal{N}(\sigma_0)$ result in the same formula that has been called the Limited Power Law (LPL)

$$\Lambda(t) = \frac{A\left(\gamma(q, \lambda_b t) - \gamma(q, \lambda_a t)\right)}{t^q}. \tag{5}$$

In this formula, t is the elapsed time since the mainshock, A is a constant,

$$\gamma(\rho, x) = \int_0^x \tau^{\rho-1} \exp(-\tau)\, d\tau,$$

is the incomplete Gamma function, and λ_b and λ_a are two characteristic aftershock rates (Fig. 1a):

- $\lambda_b = \lambda(\sigma_b)$ corresponds to an upper bound on the overload distribution ($\mathcal{N}(\sigma_o > \sigma_b) = 0$).
- $\lambda_a = \lambda(0)$ corresponds to a threshold of crack growth at low stress level for which strengthening processes may dominate, and prevent the propagation of the rupture [*Cook*, 1986].

In this model, a large range of power law decay rates result from different shapes of $\mathcal{N}(\sigma_0)$ and $\lambda(\sigma_0)$ (see example with $q = 1$ in Fig. 1, and *Narteau et al.* [2002] for examples with $q < 1$ and $q > 1$ associated with exponential and power law shape of

$\lambda(\sigma_0)$ respectively). However, the main characteristic of the LPL is to limit the power law aftershock decay rate by an exponential regime over long time $t > t_a$ ($t_a \sim 1/\lambda_a$) and a linear decay rate over short time $t < t_b$ ($t_b \sim 1/\lambda_b$). Transition from one regime to another can be related to physical properties of the brittle layer where the aftershock sequence takes place. First, in *Narteau et al.* [2002] and *Narteau et al.* [2003], we have shown that the exponential cutoff in the power-law scaling over long time could be related to structural properties of the fractured medium. Second, over short time, the time delay before the onset of the power law regime can be directly estimated from the upper limit of the overload distribution ($\sigma_b \rightarrow \lambda_b \rightarrow t_b$ as illustrated in Fig. 1a). It follows that assuming $q = p = 1$ and $\lambda_a \rightarrow 0$ in Eqs. 1 and 5 (this is the case in Fig. 1a), we have

$$c = \frac{K}{A\lambda_b} \tag{6}$$

at $t = 0$. In this study, we will work under such conditions to link the LPL to the MOL and to discuss at any stage either the λ_b value or the c value in relation with the σ_b value (Fig. 1b).

What is the physical meaning of this upper limit of the overload distribution in the brittle crust? Locally, where the rupture stops, compositional and structural heterogeneities are probably playing an important role in maintaining the stress level below the yield strength of the rock [*Wesnousky*, 2006]. In addition, aftershocks are expected to occur preferentially on pre-existing fractures distributed over a wide area. Therefore, the aftershock generation process may not be dictated only by the complexity of earthquake slip and microscopic details of the stress redistribution in the vicinity of the rupture tips. It may also depends on prestress patterns and time-dependent behaviors of a discrete population of fractures further away from the rupture. Taking a step function with a

maximum threshold (Fig. 1), we model such a population of seismic sources that have not broken during the mainshock event by following the degradation of their strength over time due to stress. Hence, the rupture is delayed according to a minimum time delay which represents the remaining strength. Such a delay is likely to be highly dependent on the magnitude thresholds for mainshocks and aftershocks [*Shcherbakov et al.*, 2004] and, for the specific implementation developed below, this is why we focus only on large aftershocks of intermediate size mainshocks.

The main idea behind our analyzes is that, at a regional length scale, when averaged on a representative sample of aftershock sequences triggered by mainshocks in the same magnitude range, the variation of the upper limit of the overload distribution should reflect variation in the load (i.e. in the mean value of the overload distribution itself). This load being essentially affected by the tectonic motions and major seismic or aseismic events, the evolution of a spatially averaged σ_b value (expressed by either λ_b or c) could allow for a better understanding of the accommodation of deformation along plate boundary. One more time, large magnitude earthquakes producing higher stress perturbations, temporal variations of the σ_b value due to the tectonic loading is more likely to be isolated if we are only studying small magnitude events. Dealing with seismological constrains, let us now present how we try to estimate such a macroscopic parameter from the catalogs of seismicity.

3. The average aftershock decay rate within the first day

We extract mainshocks from the U.S. Advanced National Seismic System ($ANSS$) composite catalog according to the algorithm of *Gardner and Knopoff* [1974] (Tab. 1). Then, we select $M_M^{Min} < M < M_M^{Max}$ mainshocks, but events preceding over 10 days an

earthquake of a magnitude greater or equal at a distance shorter than 50 km are excluded from consideration as potential foreshocks. For all the remaining mainshocks, we record the corresponding aftershock sequence within 1 *day* and a 40 *km* diameter circle.

In order to avoid artifacts arising from overlapping records, we do not consider large earthquakes and their aftershocks sequences. Thus, we essentially analyze events outside what is usually called the aftershock zone of largest events [*Wiemer and Katsumata*, 1999]. We only deal with intermediate magnitude mainshocks, $M_M^{Min} = 2.5$ and $M_M^{Max} = 4.5$, considering that their $M > M_A^{Min}$ aftershocks are likely to be detected for two main reasons: first,

$$M_\Delta = M_M^{Max} - M_A^{Min} \tag{7}$$

is small and aftershocks under consideration are always relatively large in comparison to their mainshocks [*Utsu et al.*, 1995]; second, they are not in the zone of highest seismicity when they occur. Most importantly, using intermediate magnitude mainshocks, they are distributed in the entire seismic zone and the resulting catalog of aftershocks is the best available sampling of the seismicity of an entire area for a given period of time.

3.1. Statistical properties of selected aftershocks

In this section, we study the statistical properties of aftershocks that have been selected by our procedure starting with $M_A^{Min} = 1.0$. Overall, we try to verify that the frequency-size distributions of the selected aftershocks respect the *Gutenberg and Richter* [1944] relationship

$$\log_{10} N = a + bM \tag{8}$$

where M and N are the magnitude and the number of earthquakes respectively. The b value is estimated by a maximum likelihood method in a magnitude range which depends on M_c, the magnitude of completeness of the catalog. This magnitude of completeness is evaluated according to the procedure suggested by *Wiemer and Wyss* [2000] using a threshold of 10% for the residual fit between observed and predicted cumulative number of events. This method consists in estimating the b value in the magnitude range $[M_{Min}; M_{Max}]$ for an increasing M_{Min} value. Then, taking $M_{max} = 3.4$, the M_c value is determined by the lowest M_{Min} value for which 90% of the observed data are modeled by a straight line fit according to Eq. 8.

In the following, different catalogs of aftershocks compiled in:

- Central California from 1984 to 2005.
- Central California from 1991 to 1994.
- Central California from 2001 to 2004.
- along the SAF from 1984 to 2005.

are analyzed with the same methods (see aftershocks in Fig. 2).

Fig. 3(a) shows for each of these catalogs the cumulated and non-cumulated frequency-size distributions as well as the maximum likelihood fit of the cumulated frequency-size distribution. Fig. 3(b) shows the magnitude of aftershocks and the magnitude of completeness for logarithmic time periods with respect to the time from mainshocks (i.e. time periods with the same width in logarithmic scale). In all cases, $M_c \leq 1.8$ despite some fluctuations due to the small number of events over short time. In addition, frequency-size distributions exhibit a power-law behavior which is almost the same in all catalogs.

Fig. 4 shows the cumulated and non-cumulated frequency-size distributions as well as the maximum likelihood fit for logarithmic time periods with respect to the time from mainshocks. The power-law regime is persistent over short time, and the b value is in a vast majority of cases stable over the different time periods despite the difference in the number of aftershocks under consideration.

From the comparison between Fig. 3 and Fig. 4, we conclude that the catalogs of aftershocks obtained by our selection procedure does not exhibit systematic bias due to the incompleteness of catalogs for $M \geq 1.8$. Furhtermore, these figures show that the slope of the frequency-magnitude relationship is not only stable in different subregions over various time periods but also stable over logarithmic time period after the mainshock. Consequently, as in *Narteau et al.* [2005], $M_A^{Min} = 1.8$ and $M_\Delta = 2.7$ are used as default values in our procedure of aftershock selection.

3.2. Estimation of the time delay before the onset of the power law decay rate

Using a M_A^{Min} value determined above, our procedure of selection is repeated every two months to past events occurring over a period of two years (i.e. sliding windows of $\Delta T_w = 2\ yrs$ with time shift of 2 months). Then all aftershock sequences are stacked by sorting each event according to the time interval from its respective mainshock. Artifacts resulting from catalog compiler overload should be significantly attenuated when averaged over such a long time. Similarly, administrative and technical artifacts can be considered as noises of different natures which should have a smaller influence as far as the sequences are stacked over a long period of time and a large area. Nevertheless, as a variable at time t is estimated from events occurring in $[t - \Delta T_w; t]$, the response to a perturbation may

be shifted forward in time, particularly if there is not a significant increase in seismicity associated with such a perturbation (i.e. low number of new selected aftershocks).

Before coming to the estimation of the parameters of the MOL and the LPL, we emphasize a fundamental feature of the model: the spatial distribution of the selected mainshocks is broad and covers the entire fault system under consideration (Fig. 5); furthermore, before and after a large earthquake, distributions of selected mainshock exhibit strong similarities despite a densification of seismicity around the rupture (Fig. 5a). Hence, we are always analyzing a macroscopic property on a disperse population of seismic events.

As shown in Sec. 2 for an individual sequence, the power law regime of the LPL results from a large number of exponential decay rates which overlap with one another according to the overload distribution just after the mainshock (see Eq. 4). On the basis of this summation, combining different aftershock sequences in a stack is a natural and relevant extension of this model to the description of the state of stress and strength of an entire seismic zone.

By selecting aftershocks through our time window approach, we end up with a bimonthly average aftershock decay rate over one day and we investigate the onset of the power law regime. From the stacked catalogs with more than 40 events, a best-fitting procedure using the method of maximum likelihood is devoted to estimating the parameters $\{K, c, p\}$ of the MOL (Eq. 1) and the parameters $\{A, q, \lambda_a, \lambda_b\}$ of the LPL (Eq. 5). For a sequence with N aftershocks occurring at time t_j, $j \in [1, ..., N]$ within a $[t_1, t_2]$ time interval, the maximum likelihood function for Eqs. 1 and 5 is

$$L = \exp\left(-\int_{t_1}^{t_2} \Lambda(t)dt\right) \prod_{i=1}^{N} \Lambda(t_i).$$

In more details, parameters are estimated via a method of continuous minimization by simulated annealing (*Press et al.*, 1992), which is more likely to converge to the global maximum, rather than hitting a local one by accident. As said above, we consider $p = q = 1$ and $\lambda_a \to 0$ (Fig. 1) in order to facilitate the evaluation of c values and λ_b values (see Eq. 6) as well as the comparison between each of these parameters over different time periods.

4. The onset of the power law regime across the San Andreas fault system

As an example of the data we are dealing with, Fig. 6 shows the average aftershock decay rates over six different periods of time and the best fit provided by Eqs. 1 and 5. Before interpretation of these results, the quality of fit of the MOL and the LPL may also be quoted. In fact, despite the relationship between c and λ_b when $t \to 0$, the LPL and the MOL does not behave identically. Then, without fixed parameter, we compare these models by calculating ΔAIC values, the difference between their Akaike Information criterion

$$AIC = 2n_p - 2\max\{\ln(L)\},$$

where n_p is the number of parameter for a given model (3 for the MOL and 4 for the LPL). For all time periods since 1985 in southern California, Fig. 7 shows that most of the time the LPL fits the data better than the MOL despite an additional parameter (i.e. $\Delta AIC = AIC_{LPL} - AIC_{MOL} < -2$). More than the power law regime and the linear regime, the main advantage of the LPL is to provide a better estimation of the aftershock rate during the transition from one regime to another. Such a transition is the cornerstone of the present paper, and, in the following, we will focus on the evolution of λ_b and its correlation with patterns of seismicity (Fig. 8).

4.1. Southern California

Let us first recall some results obtained for earthquakes located in southern California between 31^o and 35^o North, and 240^o and 246^o Est over the last 20 yrs (Fig. 5). *Narteau et al.* [2005] observed that λ_b suddenly decreases after large earthquakes, and slowly increases at a constant rate during periods of low seismicity (Fig. 8a). This observation was verified at smaller length scales of few hundreds of km in the neighborhood of the Landers, Northridge, and Hector Mine mainshocks. Whence, these asymmetric behaviors has been be related to the seismic cycle picture and, using the correlation with the Benioff strain accumulated over the moving time window (see Fig. 4a in *Narteau et al.* [2005]), characteristic patterns of loading and discharge have emerged:

1. During interseismic periods, the tectonic forcing increases the load within the system. As a result, σ_b, the upper limit of the pertubations induced by $2.5 < M < 4.5$ earthquakes is always increasing at the same rate in logarithmic scale ($\log_{10}(\lambda_b) \sim t/t_0$ with $t_0 \approx 2.78\ yr$), and the delay before the onset of the power law decay rate is decreasing (i.e. λ_b value increases).

2. After a large earthquake, dissipation, relaxation and stress transfer processes are associated with the rupture and its aftermath [*Nur and Booker*, 1972; *Deng et al.*, 1999]. Almost immediately, σ_b, the upper limit of the pertubations induced by $2.5 < M < 4.5$ earthquakes collapses to a smaller value, and the delay before the onset of the power law decay rate is increasing (i.e. λ_b value decreases).

Are these observations similar and these inferences valid northward where the SAF system and the seismicity exhibit different types of structural and spatiotemporal patterns?

4.2. Central California

In central California, in order to avoid complexities arising from slip partitioning between the SAF and the Calaveras fault, we analyze only earthquakes located south of the branching point (the central California zone in Fig. 9a). In this region, Fig. 6 shows that the time delay before the onset of the power law decay rate is not constant, but increases, at least since 1993. For the last 20 years, the evolution of the λ_b value has some characteristic features which can be compared to the Benioff strain in Fig. 8b. In addition, Fig. 9d shows the evolution of λ_b value on a smaller region centered on the SAF (the SAF zone in Fig. 9a). The comparison between Figs. 9c and 9d shows that major behaviors of the λ_b value are stable and originate from the SAF. Unfortunately, such more detailed analysis are impossible anywhere else in central California because of a smaller density of seismic events outside of the SAF zone. In the appendix, we explore the parameter space of the aftershock selection procedure to give the opportunity to evaluate the statistical significance of the behaviors observed below in Fig 9. In particular, we show that all the results discussed below remain for more constraining declustering methods and magnitude thresholds for mainshocks and aftershocks.

Starting from a relative small value, λ_b is continuously increasing between 1987 and 1990 ($\log_{10}(\lambda_b) \sim t/t_0$ with $t_0 \approx 6.67\ yr$ in Fig. 9c and $t_0 \approx 11.1\ yr$ in Fig. 9d), before it reaches a plateau. This relatively high value is conserved for 4 years at a regional length scale. In the SAF zone, the λ_b value continues to increase at the same rate. At the beginning of 1995, the λ_b value starts to decrease at a constant rate until the end of 1998 ($\log_{10}(\lambda_b) \sim -t/t_0$ with $t_0 \approx 4.76\ yr$ in Fig. 9c and $t_0 \approx 3.23\ yr$ in Fig. 9d). Then, another plateau is reached until the San Simeon and the Parkfield earthquakes, the 22^{nd} of

December 2003 and the 28^{th} of December 2004 respectively. Simultaneously, the Benioff strain accumulated over the 2 years time window is constant, except for a constant decay rate before 1990, and the San Simeon and Parkfield earthquakes which result in a step increase.

Some of these behaviors reinforce the hypothesis that the evolution of the λ_b value is strongly dependent on seismic discharge and, in some way, correlated to the unloading rate across the SAF system:

1. the constant increase rate between 1988 and 1990 correspond to a period of time with very low seismicity ($M < 4$).

2. the plateau between 1991 and 1995 is associated with a series of $3 < M < 5$ earthquakes, especially in the vicinity of Middle Mountain.

3. the collapse of the λ_b value is associated with the San Simeon and the Parkfield earthquakes.

Nevertheless, between 1995 and 1998, the constant decrease rate cannot be associated with any seismic pattern. Is this feature related to another type of discharge mechanism?

In fact, across the SAF system in central California, the moment rate calculated from the slip rate distribution can not be neglected when compared to the moment rate calculated from seismic events. Furthermore, during the 1990's, if the seismicity is relatively low in central California, the seismic behavior along the SAF is evolving and, following *Langbein and Hart* [1999], transient slip events have been quantitatively identified and measured by different groups.

From the analysis of more than a decade of high quality data, particularly those from the two-color electronic distance meter in the Parkfield area, *Gao et al.* [2000] suggest

that the SAF underwent two transient phases of slip summarized in Tab. 2: a transient decrease in slip rate of about 1.5 $mm.yr^{-1}$ from 1991 to 1993; a transient increase in slip rate of about 3.3 $mm.yr^{-1}$ from 1993 to 1998. The standard deviation associated with the slow down of the slip rates makes the observation much more controversial than the subsequent increase. *Langbein and Hart* [1999] and *Gao et al.* [2000] note that this increase of slip rate occur just after a sequence of $3 < M < 5$ earthquakes in the vicinity of Middle Mountain, but last for few years afterward.

Recently, such a triggering has been also identified by a time-dependent inversion done by *Murray and Segall* [2005]. More importantly, this work have provided a new set of informations about spatiotemporal properties of aseismic deformation on the SAF at Parkfield. Spatially, from a model of a fault plane of 40 km long with a seismogenic depth of 14 km, they have shown that the slip rate may have reached 49 $mm.yr^{-1}$ northwest of Carr Hill. This slip rate is not only higher than the slip rate of 15 $mm.yr^{-1}$ predicted between 1986 and 1990 but also higher than the long-term geological rate of 39 $mm.yr^{-1}$ between the American and Pacific plates. Temporally, *Murray and Segall* [2005] limit the period of high slip rate from October 1992 to July 1996 (Fig. 9b). The moment release during this time period is equivalent to a M_w5.6 earthquake, a major event for this segment of the SAF. Then, they conclude that the transient aseismic event relaxed more slip than required to dissipate the stress perturbation induced by the triggering seismic events. Thus, the transient slip corresponds to an effective release of the strain stored along the SAF.

These results inferred from geodetic observations can be straightforwardly correlated with the evolution of the λ_b value:

1. The acceleration of the slip rate observed by *Gao et al.* [2000] overlaps almost completely with the constant decay rate of the λ_b value (Fig. 8b and Tab. 2). Indeed, the λ_b values estimated from time windows encompassing only earthquakes that occurred during the period of higher slip rate (i.e. 1993-1998) extend from 1995 to 1998 (i.e. the time period during which the decrease is the most significant).

2. As shown in Figs. 9c and 9d, we can observe than the short period of high slip rate determined by *Murray and Segall* [2005] triggers the decrease of the λ_b value. As above, taking into account the duration of the time window, the transient slip rate is synchronized with the decrease of the λ_b value. Similarly, during a short period of low seismicity (i.e. $M < 4$), a constant increase rate of the λ_b value between 1987 and 1990 corresponds to a constant slip rate of approximately 15 $mm.yr^{-1}$.

More generally, from the comparison between Fig. 8a and Fig. 8b we can observe that, in average, the λ_b value is higher in central California than in southern California. In addition, the logarithmic slope of the variation of the λ_b value is always lower in central California than in southern California.

Since the characteristics of fatigue failures may be related to a given rheology, all the behaviors exposed above in term of load can be translated in terms of stress and strain.

5. Stress changes and loading rates inferred from aftershocks

Fig. 10 illustrates schematically how a mean value of the overload distribution, i.e.

$$\mu_{\sigma_0} = \int_{-\infty}^{\infty} \sigma_0 \mathcal{N}(\sigma_0) d\sigma_0,$$

can be related to the the upper bound σ_b of the overload distribution at the length scale of the $2.5 < M < 4.5$ mainshocks that we are considering. In addition, it shows how, the

μ_{σ_0} value could evolve according to different modes of deformation in the upper crust of the Earth.

Based on Fig. 10, let us discuss the loading rates in the framework of the LPL model (Fig. 1a). If $\lambda(\sigma_0)$ is an exponential transition rate, and $\lambda_b = \lambda(\sigma_b)$, the gradual increase of the λ_b value in southern California during interseismic periods can be related to a constant increase of the σ_b value

$$\sigma_b(t) \sim \alpha t. \tag{9}$$

Assuming uniform strength over the entire population of domains, this upper limit of the overload distribution is proportional to an absolute level of differential shear stress (i.e. μ_{σ_0} in Fig. 10). For a linear elastic rheology, it follows that the rate α in Eq. 9 can be related to a strain accumulation rate. In other word, we conclude that, in stick-slip zone, the time derivative of the logarithm of the λ_b value is proportional to the interseismic strain accumulation rate (Fig. 10).

Applied to central California, where aseismic slip accommodates a more significant part of the deformation, we find that the maximum strain accumulation rate between 1987 and 1990 is approximately three times lower than in southern California (see the constant slopes of $\lambda_b(t)$ in Figs. 9c and 9d). From 1991 to 1993, a plateau of $\lambda_b(t)$ tends to indicate a balance between strain release and strain accumulation rates. Later, strain release dominates, through aseismic deformation between 1995 and 1998, then through two major seismic events for this region (San Simeon and Parkfield earthquakes). Therefore, we conclude that, in creep-slip zone, the time derivative of the logarithm of the λ_b value is not only proportional to the strain accumulation rate but also inversely proportional to the strain release rate (Fig. 10).

Coupled with a model of interseismic deformation, the behaviors of the λ_b value could provide more quantitative assessments of the stress changes in central California. From the exponential transition rate presented in Fig. 1a, we have

$$\frac{d\,\log_{10}(\lambda_b)}{d\,t} = \frac{1}{\log(10)\sigma_a}\,\frac{d\,\sigma_b}{d\,t} \tag{10}$$

On the other hand, for a linear elastic rheology, we can write

$$\frac{d\,\sigma}{d\,t} = G\dot{\epsilon},$$

where $d\,\sigma/d\,t$, $\dot{\epsilon}$ and G are the variation rate of the differential shear stress, the shear strain accumulation rate, and the shear modulus respectively. By considering a simple screw dislocation model with a vertical strike-slip fault locked at depth D, *Savage and Burford* [1973] suggested that, on the free surface and following x, the distance perpendicularly to the fault, the shear strain accumulation rate can be related to a deficit of slip rate v_s by

$$\dot{\epsilon} = \frac{v_s\ D}{2\pi(x^2 + D^2)}.$$

It follows that

$$\frac{d\,\sigma}{d\,t} = \frac{G\ v_s\ D}{2\pi(x^2 + D^2)}. \tag{11}$$

After the substitution of the time derivative of the differential shear stress (Eq. 11) into Eq. 10, we obtain

$$\frac{d\,\log_{10}(\lambda_b)}{d\,t} = \frac{G\ D}{2\pi\log(10)\ \sigma_a(x^2 + D^2)}v_s. \tag{12}$$

This equation gives the opportunity to relate the results exposed in Figs. 8 and 9 to different measures of slip rates across the SAF system.

Summarized in Tab.3, let us discuss one by one the 6 points that we can derive from the evolution of the λ_b value (see the t_0 value in Sec. 4 and in Fig. 9) and from the slip rate inferred from geodetic data.

At a regional length scale, $W \approx 200\ km$, three significant trends in the variation of the logarithm of the λ_b value can be estimated:

1. During interseismic periods in southern California, $d\log_{10}(\lambda_b)/dt = 0.36\ yr^{-1}$. Meanwhile, the slip rate is assumed to be zero, the deformation being essentially accommodated by seismic events. As a consequence, the deficit of slip rate is given by the long-term geological slip rate.

2. From 1987 to 1990 in central California, $d\log_{10}(\lambda_b)/dt = 0.15\ yr^{-1}$. Meanwhile, the maximum slip rate along the SAF has been estimated at 15 $mm.yr^{-1}$ by *Murray and Segall* [2005].

3. From 1995 to 1998 in central California, $d\log_{10}(\lambda_b)/dt = -0.21\ yr^{-1}$. Meanwhile, the maximum slip rate along the SAF has been estimated at 49 $mm.yr^{-1}$ by *Murray and Segall* [2005].

For all these cases, the long-term geological slip rate is taken equal to 39 $mm.yr^{-1}$, the angular velocity that best describes motion of the Sierra Nevada Great Valley block relative to the Pacific plate [*Argus and Gordon*, 2001]. At a smaller length scale of $W \approx 1\ km$ in the vicinity of the SAF near Parkfield (see the SAF zone in Fig. 9), two significant trends in the variation of the logarithm of the λ_b value can be estimated:

4. From 1987 to 1990, $d\log_{10}(\lambda_b)/dt = 0.09\ yr^{-1}$. As said above, during this time interval, the maximum slip rate along the SAF has been estimated at 15 $mm.yr^{-1}$ by *Murray and Segall* [2005].

5. From 1995 to 1998 in central California, $d\,\log_{10}(\lambda_b)/d\,t = -0.31\ yr^{-1}$. As said above, during this time interval, the maximum slip rate along the SAF has been estimated at 49 $mm.yr^{-1}$ by *Murray and Segall* [2005].

For all these cases, the long-term geological slip rate is taken equal to 28 $mm.yr^{-1}$, as suggested by *Titus et al.* [2005] from continuous GPS measurements between pairs of sites that flank the creeping segment at intersite distances of 1 km.

Furthermore, we consider the null hypothesis.

6. For slip rates equal to the long-term geological slip rate, the deficit of slip rate is null, and we consider that $d\,\log_{10}(\lambda_b)/d\,t$ is equal to zero.

Gathering all these points together, Fig. 11 shows the relationship between $d\,\log_{10}(\lambda_b)/d\,t$ and the deficit of slip rate v_s. There is a clear linear relationship, and the best fit straight line of slope $s = 0.0105\ mm^{-1}$, obtained by regression, is also shown on the figure. Such a positive slope confirms that the evolution of the λ_b value is likely to result from variations in the load of the brittle upper crust.

From Eq. 12, we have

$$s = \frac{G\ D}{2\pi \log(10)\ \sigma_a (x^2 + D^2)}. \tag{13}$$

It follows that, if no deformation is accommodated on different faults or on off-fault structures, the normalizing stress constant σ_a can vary with respect to the distance to the SAF. Then,

$$\sigma_a = \frac{G\ D}{2\pi \log(10)\ s\ (x^2 + D^2)}. \tag{14}$$

From this equation and the exponential expression of $\lambda(\sigma_0)$, we can simply quantify stress variations within the upper crust, $\Delta\sigma_b$, in response to change in the λ_b value:

$$\Delta\sigma_b = \sigma_b(t+\Delta t) - \sigma_b(t) = \sigma_a \log\left(\frac{\lambda_b(t+\Delta t)}{\lambda_b(t)}\right) = \frac{G \log_{10}\left(\frac{\lambda_b(t+\Delta t)}{\lambda_b(t)}\right)}{2\pi\ s\ D\ \left(\left(\frac{x}{D}\right)^2 + 1\right)}. \quad (15)$$

For example, for the gradual decrease of the λ_b value along the SAF near Parkfield from 1995 to 1998 (Fig. 9d), we have $\lambda_b(t+\Delta t)/\lambda_b(t) = 0.1$. Then

$$\begin{array}{llll} \Delta\sigma_b = -0.32 & bars & \text{for} & x = 0\ km. \\ \Delta\sigma_b = -0.16 & bars & \text{for} & x = 14\ km. \\ \Delta\sigma_b = -0.07 & bars & \text{for} & x = 28\ km. \\ \Delta\sigma_b = -0.01 & bars & \text{for} & x = 78.5\ km. \end{array}$$

with $G = 3\ 10^5\ bars$, $D = 14\ km$, $s = 0.0105\ mm^{-1}$ (see Fig. 11).

Far from the fault, our estimation is on the same order of magnitude than Coulomb stress changes induced by $M \approx 6.5$ earthquakes like Coalinga or San Simeon earthquakes over the same distances. In the vicinity of the SAF, the change in stress due to the transient slip event is on the order of magnitude of the lower range limit of earthquake stress drop [*Hanks*, 1977]. This stress variation is also consistent but smaller with observation of low stress drop events at a border between locked and creeping fault patches [*Sammis and Rice*, 2001]. As the $\Delta\sigma_b$ value is representative of a change in stress average over an entire volume within which the aftershocks take place, it is likely that locally variation of stress can be much larger especially along pre-existing fractures and discontinuities. However such a value of 0.3 $bars$ is already significant. Indeed, a discharge rate of 0.1 $bars.yr^{-1}$ (0.3 $bars$ during 3 yr) is comparable with classical estimate of the loading rate along faults. In other words, transient slip events can significantly delay the recurrence time interval for earthquakes.

From Eq. 14 and the exponential expression of $\lambda(\sigma_0)$, we can also quantify the loading rate along the SAF (i.e. $x = 0$):

$$\frac{d\,\sigma_b}{d\,t} = \frac{G}{2\pi\ s\ D}\frac{d\log_{10}(\lambda_b)}{d\,t}. \tag{16}$$

For example, in southern California, where the SAF is not creeping and where $d\log_{10}(\lambda_b)/dt = 0.36\ yr^{-1}$, we obtain a loading rate equal to 0.117 $bar.yr^{-1}$. For this region, paleoseismic and geological observations have shown that the mean recurrence time of major events along the SAF is about 250 yr [*Sieh*, 1984]. Over such an interseimic period, the loading rate estimated above yields to a change in stress of about 30 $bars$. This value is in good agreement with stress drop associated with large interplate earthquakes [*Scholz*, 1990].

These numerical investigations demonstrate that our method, which is only based on the examination of the aftershock decay rate and on geodetic measurements, can lead to realistic evaluations of stress variations and loading rates within the brittle upper crust. Hence, the evolution of the λ_b value may provide useful informations for recognized characteristic patterns of strain accumulation and release across seismic and aseismic fault systems.

6. Discussion and conclusion

It is likely that earthquakes are strongly under-reported during early parts of aftershock sequences, and the c value may be significantly influenced by non-physical effects. Unfortunately, it is impossible to answer the question of the (in)completeness of the catalogs of seismicity nowadays, despite permanently improving techniques in recording seismic waves and new types of analyzes on initial phases of seismograms. For example, here, the

λ_b value is saturated at high frequency over short time (e.g. 7 mn and 2 mn in southern and central California respectively). Nevertheless, we consider that the origin and the variation of the c value have to be examined quantitatively in relation with independent observations (e.g. the slip rate along faults). As we are aware of possible artifacts, we try to minimize them by investigating small magnitude events over a large area and stacking different aftershock sequences occurring over a long period of time. This averaging techniques is key in providing an information at the length scale of the entire fault system.

The relationship that have been suggested between the time derivative of the λ_b value and the deficit of slip rate may be tested in various type of tectonic settings worldwide. In such analysis, as in this paper, absolute values being too dependent on magnitude thresholds, only relative variations have to be investigated. Ideally, we have described a pattern of seismicity that allow for the identification of transient slip events. If if happens to be the case, it could be an opportunity to estimate acceleration or deceleration of slip across remote fault zone where geodetic measurements remains impossible.

Recently, using the same catalogs of seismicity that we use to determine the λ_b value, *Schorlemmer et al.* [2005] and *Schorlemmer and Wiemer* [2005] have suggested that the power law exponent of magnitude-frequency distributions (the b value) is directly related to the differential stresses in the Earth's crust. We analyze the aftershock decay rate to infer the same type of relationship between the delay before the onset of the power law regime and a measure of loading and unloading rates across a fault system. In addition, by comparing geodetic measurements to our seismological data, the LPL and a simple screw dislocation model allow to quantify stress variations over long times along the SAF.

We have estimate that, in southern California, where the fault is not creeping, the loading rate is on the order of 0.117 $bar.yr^{-1}$. In central California, where the fault is creeping, we have shown that changes in stress for a transient slip events are on the same order of magnitude than earthquake static stress changes. In the vicinity of the SAF the changes in stress tend to the lower limit of earthquake stress drop. Such a discharge is not instantaneous, but it occurs over a period of 3 yr along a 60 km segment of the SAF north-west of Parkfield. An estimated unloading rate of 0.1 $bars.yr^{-1}$ can compensated for an equivalent time interval of strain accumulation and then potentially delay by more than 6 yr the occurrence of the next $M6$ earthquake in Parkfield.

As a conclusion, we suggest that, the time delay before the onset of the power-law aftershock decay rate inferred from catalogs of seismicity could provide an independent constrain about loading/unloading rates across an active fault systems. In particular, if the long term geological slip rate is known, it gives an opportunity to quantify in real time strain accumulation and release rates as well as the ratio between aseismic and seismic deformation. Furthermore, stress changes in the upper crust can be evaluated according to a set of observations which do not rely on specific geometrical constraints of the fault population.

Acknowledgments

The paper was improved by the constructive comments and thoughtful suggestions of Jeffrey McGuire and two anonymous reviewers. This work was supported by E2C2, a Specific Targeted Research Project of the European Community. In the I.P.G.P., Clément Narteau benefit from a Marie Curie reintegration grant 510640-EVOROCK of the European Community.

Appendix

Fig. 12 shows the evolution of c and λ_b obtained by independent fits of the MOL and the LPL respectively in the central California zone from 1984 to 2005. As predicted by Eq. 6, the comparison between the evolution of c and $1/\lambda_b$ indicates that the MOL and the LPL give similar estimations of the time delay before the onset of the power law decay rate. Nevertheless, the aftershock decay rate for both laws can differ significantly from one model to the other especially during the transition period toward the power law regime (see Eqs. 1 and 5, and Fig. 6).

Our analysis is based on a selection procedure of aftershocks that takes few input parameters in particular for the space-time windows and the magnitude thresholds. Fig. 13 shows the effect of all these parameters on the number of selected aftershocks and on the variation of λ_b in the central California and the SAF zones from 1984 to 2005. For comparison with the results presented in Sec. 4.2, dotted lines indicate the trends that have been calculated in Fig. 9 for the periods of 1987-1990 and 1995-1998. In all figures, the quality of the fit and the stability of the results are highly dependent on the number of staked aftershocks. Experiences have shown that reliable estimates are obtained with stacks consisting of a minimum of 40 aftershocks. Note on Fig. 13 that below such a threshold, the signal that we are investigating is still present but with a significant increase in the noise level (this is, most of the time, the black curves).

In order to analyze the properties of aftershock sequences over short time, a classical procedure is to eliminate events of smaller magnitude, larger events being identify more easily in seismograms. Then, according to *Utsu et al.* [1995], a time delay before the onset of the power law aftershock decay is not an artifact if this time delay converges to

a constant value for an increasing M_A^{Min} value. Here, given our procedure of selection with magnitude thresholds for mainshocks and aftershocks, such a test can be done by decreasing the M_Δ value (Eq. 7). Hence, Fig. 13a shows the evolution of λ_b for a fixed M_A^{Min} value and a decreasing M_M^{Max} value, as well as for a fixed M_M^{Max} and an increasing M_A^{Min} value. For $M_\Delta \in [1.6; 2.6]$, all curves collapse onto the curve obtained with the default values (see Fig. 9c and 9d where $M_A^{Min} = 1.8$, $M_M^{Max} = 4.5$) despite strong fluctuations when the number of aftershocks in the stack is too low. These results indicate that there is no significant bias associated to the magnitude thresholds in our catalogs of aftershocks. We emphasize that it is because we only using the largest event of intermediate magnitude mainshocks (minimization of M_Δ).

Fig. 13b shows the evolution of λ_b for different duration of the time window, keeping a time step of two months. The main characteristic of a time window is to reduce the level of noise by averaging a number of consecutive measurements over time. Hence, not surprisingly, the shorter the duration of the time window, the higher the level of noise. This is particularly the case here since the number of events in the stack is correlated to the duration of the time window. Nevertheless, in all cases, the increase and decrease rates of λ_b remain very similar for the periods of 1987-1990 and 1995-1998 respectively.

The effect of the algorithm of *Gardner and Knopoff* [1974] (Tab. 1) is tested by multiplying and dividing the space-time windows by 2 and 3 respectively (Fig. 13c). Reducing windows by a factor 3 diminishes the number of aftershocks in the stacks and consequently increases the variability of the signal. Increasing the windows by a factor 2 has no impact on the result because the probability to have an uncorrelated $M > M_A^{Min}$ earthquake during the first day remains extremely low. On the other hand, a larger number of events

in stacks offers the possibility of increasing the $M > M_A^{Min}$ value (i.e. of decreasing the M_Δ value). In this case also, the evolution of λ_b is almost the same as in Figs. 9c and 9d, and, interestingly, much more stable than the curve with the same magnitude thresholds in Fig. 13a (i.e. the black with $M_A^{Min} = 2.2$, $M_M^{Max} = 4.5$).

Finally, we modify our technique of selection itself. The algorithm of *Gardner and Knopoff* have only been used to select mainshocks, but, for the selection of aftershocks, the space windows scale with the magnitude M of the mainshock. Practically, we consider a circular area with a radius

$$R = 10^{\beta(M - M_M^{Min})}\, r,$$

where β is a constant, and r is an arbitrary distance. Fig. 13d shows the evolution of λ_b for a fixed β value and different r values, and for a fixed r value and different β values. It shows also the results from catalogs of aftershocks obtained by taking the spatial parameters of the *Reasenberg* [1985] declustering method ($\beta = 0.41$, $r = 1.12\ km$). All curves behaves similarly but for the largest r value in the SAF zone, aftershocks are mixed with significant uncorrelated seismicity along the fault, and this starts to affect the temporal decay of aftershock rate over time (green curve in Fig. 13d). The *Reasenberg* [1985] parameters gives a smaller number of events than our default procedure but the shape of the evolution of λ_b persists.

From Fig. 13, we can conclude that, considering large aftershocks of intermediate size mainshocks (small M_Δ value), it is possible to capture time variations of the λ_b parameter. However, a strong constrain comes from the number of aftershocks in the stacks. This number has to be larger than 40 to ensure the quality of fit of the MOL and the LPL and to reduce the statistical fluctuations.

References

Argus, D., and R. Gordon, Present tectonic motion across the Coast Ranges and San Andreas fault system in central California, *Geol. Soc. America Bull.*, *113*, 1580–1592, 2001.

Atkinson, B. K., Subcritical crack growth in geological materials, *J. Geophys. Res.*, *89*, 4077–4114, 1984.

Atkinson, B. K., and P. G. Meredith, The theory of subcritical crack growth with applications to minerals and rocks, in *Fracture Mechanics of rock*, edited by B. K. Atkinson, Geology series, pp. 111–166, Academic Press, 1987.

Bennett, R. A., S. Rodi, and R. E. Reilinger, System constraints on fault slip rates in southern California and northern Baja, Mexico, *J. Geophys. Res.*, *101*, 21,943–21,960, 1996, 10.1029/96JB02488.

Charles, R., The static fatigue of glass, *J. Appl. Phys.*, *29*, 1549–1560, 1958.

Charles, R., and W. B. Hillig, The kinetics of glass failure by stress corrosion, in *Symposium on the Mechanical Strength of Glass and Ways off Improving It*, edited by B. Union Scientifique Continentale du Verre, Charleroi, pp. 511–527, 1962.

Cook, R., Crack propagation thresholds: A measure of surface energy, *J. Mater. Res.*, *29*, 862–866, 1986.

Deng, J., K. Hudnut, M. Gurnis, and E. Hauksson, Stress loading from viscous flow in the lower crust and triggering of aftershocks following the 1994 Northridge, California, Earthquake, *Geophys. Res. Lett.*, *26*, 3209–3212, 1999.

Dragert, H., K. Wang, and T. James, A silent slip event on deeper Cascadia subduction interface, *Science*, *292*, 1525–1528, 2001.

Enescu, B., J. Mori, and M. Miyasawa, Quantifying early aftershock activity of the 2004 mid-Niigata Prefecture earthquake (M_w6.6), *J. Geophys. Res.*, 2007, doi:10.1029/2006JB004629.

Fialko, Y., Interseismic strain accumulation and the earthquake potential on the southern san andreas fault system, *Nature*, *441*, 968–971, 2006.

Gao, S. S., P. G. Silver, and L. A. T., Analysis of deformation data at Parkfield, California: detection of a long-term strain transient, *J. Geophys. Res.*, *105*, 2955–2967, 2000.

Gardner, J., and L. Knopoff, Is the sequence of earthquakes in southern California with aftershocks removed poissonian?, *Bull. Seismol. Soc. Am.*, *5*, 1363–1367, 1974.

Gutenberg, B., and C. Richter, Frequency of earthquakes in California, *Bull. Seismol. Soc. Am.*, *34*, 185–188, 1944.

Hanks, T. C., Earthquake stress drops, ambient tectonic stresses ans stresses that drives plate motions, *Pure Appli. Geophys.*, *115*, 441–458, 1977.

Kagan, Y., and H. Houston, Relation between mainshock rupture process and Omori's law for aftershock moment release rate, *GeopHys. Journ. Int.*, *163*, 1039–1048, 2005.

Langbein, J., R. Burford, and L. Slater, Variations in fault slip and strain accumulation at Parkfield, California: Initial results using two-color geodimeter measurements, 1984-1988, *J. Geophys. Res.*, *95*, 2533–2552, 1990.

Langbein, J. O., Post-seismic slip on the San Andreas Fault at the northwestern end of the 1989 Loma Prieta earthquake rupture zone, *Geophys. Res. Lett.*, *17*, 1223–1226, 1990.

Langbein, R. L., J. anf Gwyther, and M. T. Hart, R. H. G.i anf Gladwin, slip-rate increase at Parkfield in 1993 detected by high precision EDM and borehole tensor strainmeters,

Geophys. Res. Lett., *26*, 2529–2532, 1999.

Murray, J. R., and P. Segall, Spatiotemporal evolution of a transient slip event on the San Andreas fault near Parkfield, California, *J. Geophys. Res.*, p. B09407, 2005.

Nadeau, R. M., and T. V. Mcevilly, Fault slip rates at depth from recurrence intervals of repeating microearthquakes, *Science*, *285*, 718–721, 1999.

Nadeau, R. M., and T. V. Mcevilly, Periodic pulsing of characteristic microearthquakes on the san andreas fault, *Science*, *303*, 220–222, 2004.

Narteau, C., Classification of seismic patterns in a hierarchical model of rupture: a new phase diagram for seismicity, *Geophys. Journ. Int.*, *168*, 710–722, 2007.

Narteau, C., P. Shebalin, and M. Holschneider, Temporal limits of the power law aftershock decay rate, *J. Geophys. Res.*, *107*, doi:10.1029/2002JB001,868, 2002.

Narteau, C., P. Shebalin, G. Zöller, S. Hainzl, and M. Holschneider, Emergence of a band-limited power law in the aftershock decay rate of a slider-block model of seismicity, *Geophys. Res. Lett.*, *30*, doi:10.1029/2003GL017,110, 2003.

Narteau, C., P. Shebalin, and M. Holschneider, Onset of power law aftershock decay rates in Soutern California, *Geophys. Res. Lett.*, *32*, doi:10.1029/2005GL023,951, 2005.

Nur, A., and J. Booker, Aftershocks caused by pore fluid flow?, *Science*, *175*, 885–887, 1972.

Omori, F., On after-shocks of earthquakes, *J. Coll. Sci. Imp. Univ. Tokyo*, *7*, 111–200, 1894.

Peltzer, G., F. Crampé, S. Hensley, and R. Rosen, Transient strain accumulation and fault interaction in the Eastern California shear zone, *Geology*, *29*, 975–978, 2001.

Peng, Z. G., J. E. Vidale, and H. Houston, Anomalous early aftershock decay rate of the 2004 mw6.0 parkfield, california, earthquake, *Geophys. Res. Lett.*, *33*, 2006.

Peng, Z. G., J. E. Vidale, M. Ishii, and A. Helmstetter, Seismicity rate immediatly before and after main shock rupture from high frequency waveforms in Japan, *J. Geophys. Res.*, *112*, 2007, doi:10.1029/2006JB004386.

Reasenberg, P., Second-order moment of central California seismicity, 1969-1982, *J. Geophys. Res.*, *90*, 5479–5495, 1985.

Sammis, C., and J. Rice, Repeating earthquakes as low-stress-drop events at a border between locked and creeping fault patches, *Bull. Seism. Soc. America*, *81*, 532–537, 2001.

Sauber, J., S. C. Solomon, and W. Thatcher, Geodetic measurement of deformation in the central Mojave Desert, California, *J. Geophys. Res.*, *91*, 12,683–12,693, 1986.

Savage, J., and R. Burford, Geodetis determination of relative plate motion in central California, *J. Geophys. Res.*, *78*, 832–845, 1973.

Schmidt, D. A., R. Bürgmann, R. M. Nadeau, and M. d'Alessio, Distribution of aseismic slip rate on the Hayward fault inferred from seismic and geodetic data, *J. Geophys. Res.*, *110*, 2005, doi:10.1029/2004JB003397.

Scholz, C., Microfractures, aftershocks, and seismicity, *Bull. Seismol. Soc. Am.*, *58*, 1117–1130, 1968.

Scholz, C. H., *The Mechanism of Earthquakes and Faulting*, Cambridge University Press, 1990.

Schorlemmer, D., and S. Wiemer, Microseismicity data forecast rupture area, *Nature*, *434*, 1086–1086, 2005.

Schorlemmer, D., S. Wiemer, and M. Wyss, Variations in earthquake-size distribution across different stress regimes, *Nature*, *437*, 539–542, 2005.

Shcherbakov, R., D. L. Turcotte, and J. B. Rundle, A generalized omori's law for earthquake aftershock decay, *Geophys. Res. Lett.*, *31*, 2004, doi:10.1029/2004GL019808.

Sieh, K., Lateral offset and revised dates of large prehistoric earthquakes at Pallet Creek, southern California, *J. Geophys. Res.*, *89*, 7641–7670, 1984.

Simpson, R. W., J. J. Lienkaemper, and J. S. Galehouse, Variations in creep rate along the Hayward Fault, California, interpreted as changes in depth of creep, *Geophys. Res. Lett.*, *28*, 2269–2272, 2001.

Titus, S., C. DeMets, and B. Tikoff, New slip rates estimates for the creeping segment of the San Andreas fault, California, *Geology*, *33*, 205–208, 2005.

Utsu, T., Y. Ogata, and R. Matsu'ura, The centenary of the Omori formula for a decay law of aftershocks activity, *J. Phys. Earth*, *43*, 1–33, 1995.

Vidale, J. E., Z. Peng, and M. Ishii, Anomalous aftershock decay rates in the first hundred seconds revealed from the Hi-net borehole data, *AGU Fall Meeting Abstracts*, pp. S51C–0170X, 2004.

Wesnousky, S. G., Predicting the endpoints of earthquake ruptures, *Nature*, *444*, 358–360, 2006, doi:10.1038/nature05275.

Wiederhorn, S., and L. Bolz, Stress corrosion and static fatigue of glass, *J. Am. Ceram. Soc.*, *50*, 543–553, 1970.

Wiemer, S., and K. Katsumata, Spatial variability of seismicity parameters in aftershock zones, *J. Geophys. Res.*, *104*, 13,135–13,151, 1999.

Wiemer, S., and M. Wyss, Minimum magnitude of completeness in earthquake catalogs: examples from Alaska, the western United States, and Japan, *Bull. Seism. Soc. Am.*, *90*, 859–869, 2000.

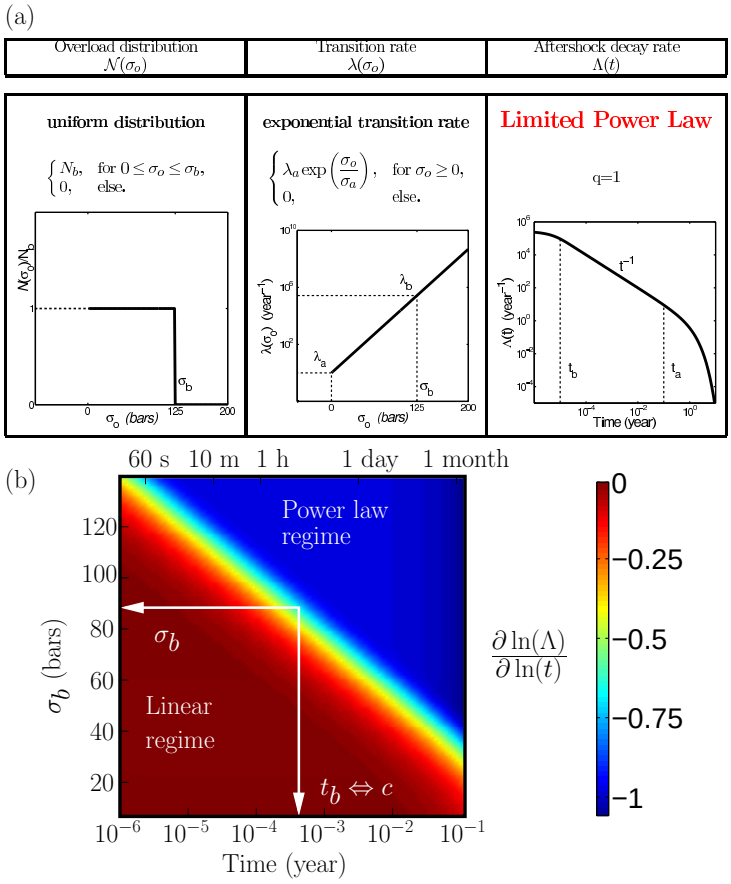

Figure 1. (**a**) A step function for the overload distribution $\mathcal{N}(\sigma_0)$ and an exponential transition rate $\lambda(\sigma_0)$ produce a limited power-law (LPL) with an exponent $q = 1$, and two characteristic aftershock rates $\lambda_b \sim t_b^{-1}$ and $\lambda_a \sim t_a^{-1}$ over short and long times respectively. We determine N_b from $\int_0^\infty \mathcal{N}(\sigma_0)d\sigma_0$. We arbitrarily choose the following numerical values: $\sigma_a = 10\ bars$, $\sigma_b = 125\ bars$, $1/\lambda_a = 1\ yr^{-1}$. Note that $\lambda_b = \lambda(\sigma_b)$. (**b**) $\partial \ln(\Lambda(t))/\partial \ln(t)$, the local slope of the LPL in logarithmic scales for σ_b values ranging from 0 to 140 $bars$, all the other parameters being kept constant. The time delay $c \sim t_b$ before the transition from a linear regime to a power law regime increases exponentially with respect to σ_b (see $\lambda(\sigma_0)$ in (a)).

$[M_{min}; M_{max}]$	L (km)	ΔT (days)
2.5-2.99	23	6
3.0-3.49	26	6
3.5-3.99	30	6
4.0-4.49	35	10
4.5-4.99	40	10
5.0-5.49	47	10
5.5-5.99	54	10
6.0-6.49	61	30
6.5-9.00	70	30

Table 1. Window algorithm for aftershocks. Note that the spatial window is larger than the original window suggested by *Gardner and Knopoff (1974)*. We verify that the L value and ΔT value do not exert significant influence over our results.

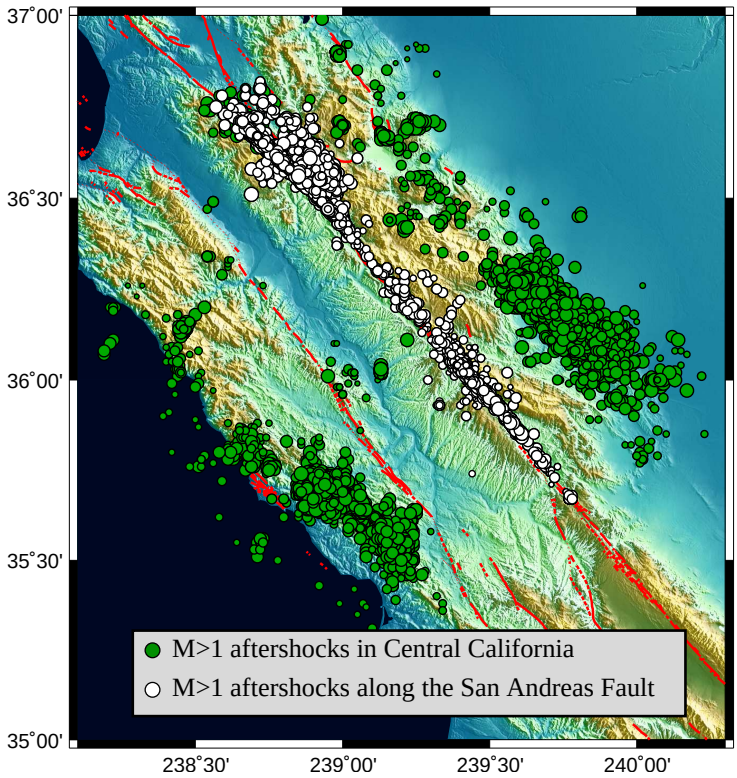

Figure 2. Selected $M > 1$ aftershocks in central California (green and white) and along the SAF (white) for the estimation of the magnitude of completeness.

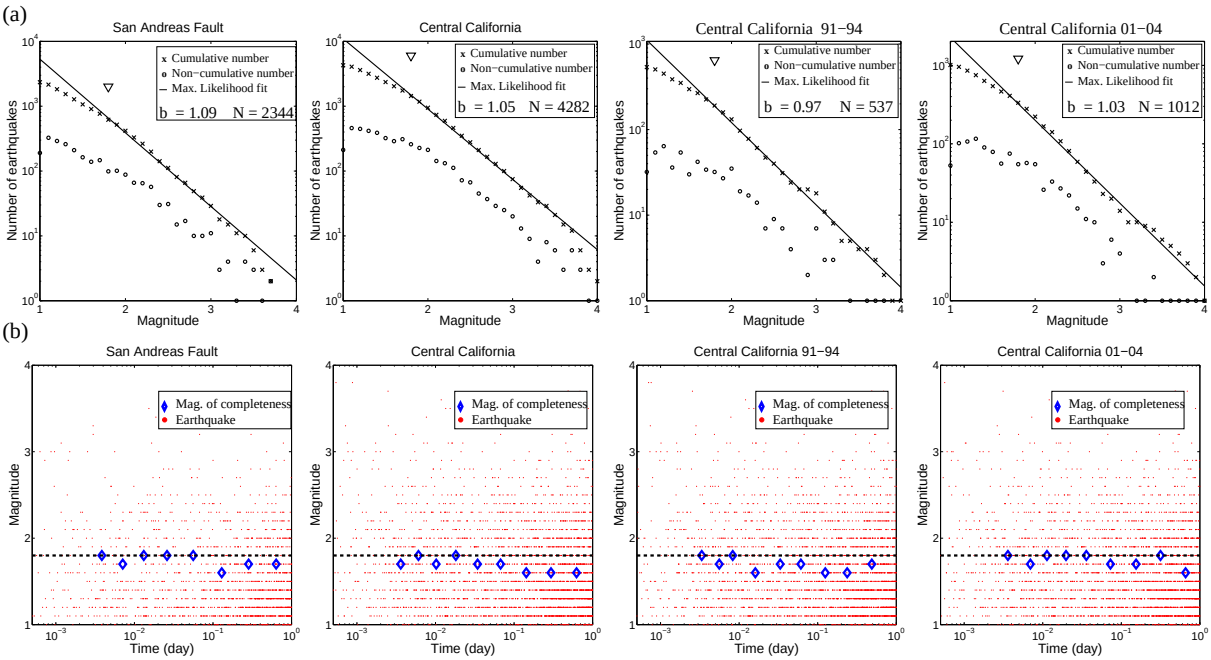

Figure 3. (a) Cumulated and non-cumulated frequency-size distributions, and the maximum likelihood fit of the cumulated frequency-size distribution. (b) Magnitude of aftershocks and the magnitude of completeness for logarithmic time periods with respect to the time from mainshocks. Triangles in (a) and dotted lines in (b) indicate the chosen minimum magnitude for aftershocks $M_A^{Min} = 1.8$. From the left to the right, the catalogs of aftershocks have been obtained along the SAF from 1984 to 2005 and in central California for the periods 1984-2005, 1991-1994 and 2001-2004 (Fig. 2).

Figure 4. Cumulated and non-cumulated frequency-size distributions, and the maximum likelihood fit of the cumulated frequency-size distribution for logarithmic time periods with respect to the time from mainshocks. Triangles indicate the chosen minimum magnitude for aftershocks $M_A^{Min} = 1.8$. From top to bottom, the catalogs of aftershocks have been obtained along the SAF from 1984 to 2005 and in central California for the periods 1984-2005, 1991-1994 and 2001-2004 (Fig. 2).

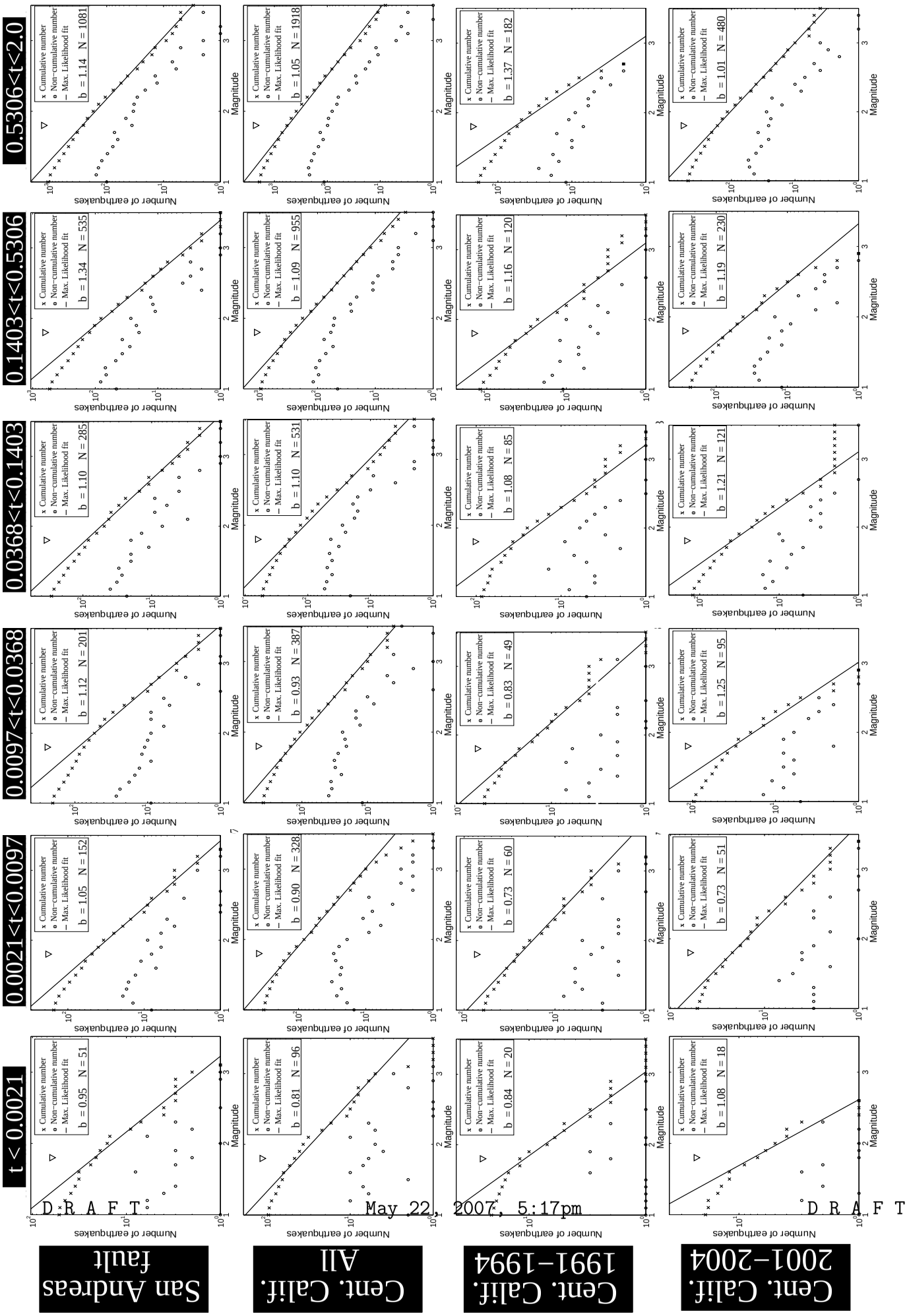

Figure 4.

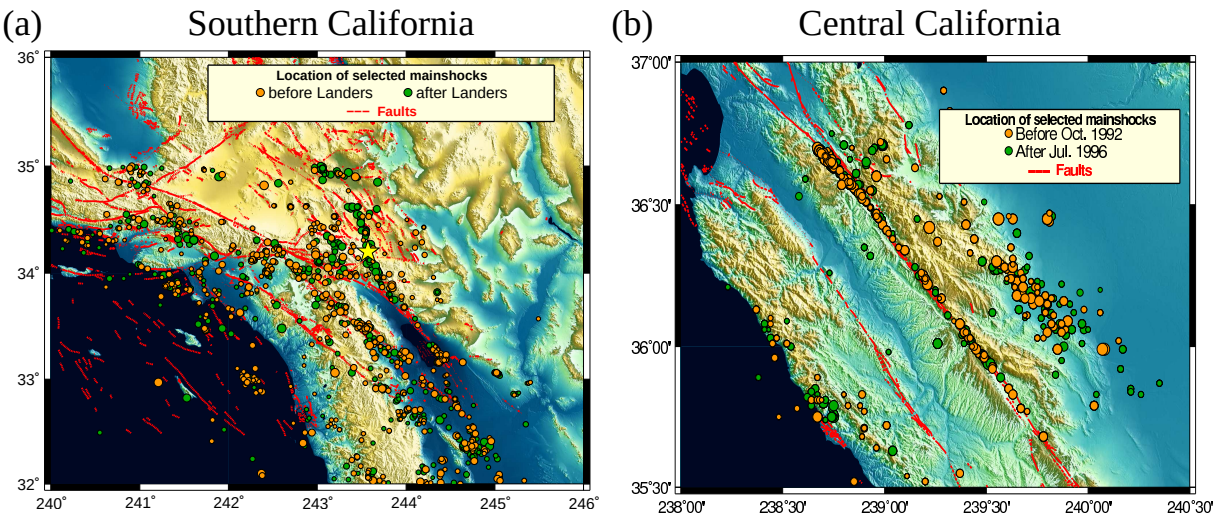

Figure 5. (**a**) In Southern California, the time delays before the onset of the power law at $t = 1992.34$ (i.e. last time window before the Landers mainshock) and $t = 1994.34$ (i.e. last time window including the Landers mainshock) are obtained by analyzing stacked aftershock sequences produced by mainshocks located under the green and the orange dots respectively. (**b**) A similar figure in central California, at $t = 1992.75$ and $t = 1996.5$, before and after a transient slip event. In each figure, note that both distributions are similar and that mainshocks are broadly distributed over the entire fault population.

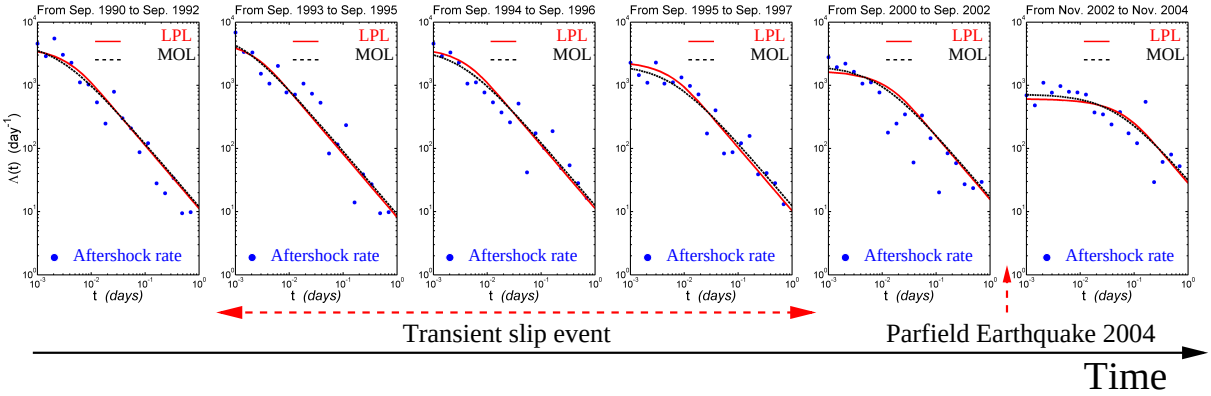

Figure 6. The average aftershock decay rate within the first day for six periods of time before and after transient slip events along the SAF and the last $M6$ Parkfield earthquake. Lines represent the best fits provided by the LPL (solid) and the MOL (dashed). Note that the increase in the time delay before the onset of the power decay rate correspond also to a decrease of the aftershock rate for $t \to 0$.

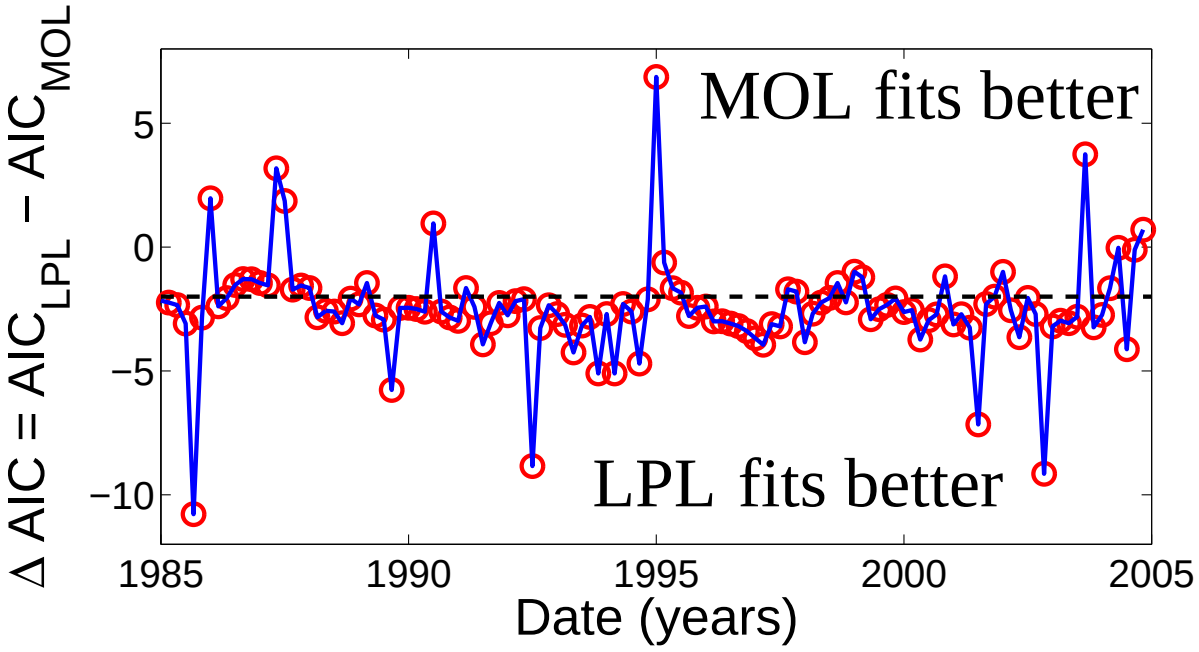

Figure 7. The difference between the AICs of the LPL and the MOL, for all the bimonthly average aftershock decay rate since 1985. The dashed line corresponds to the same quality of fit for both models.

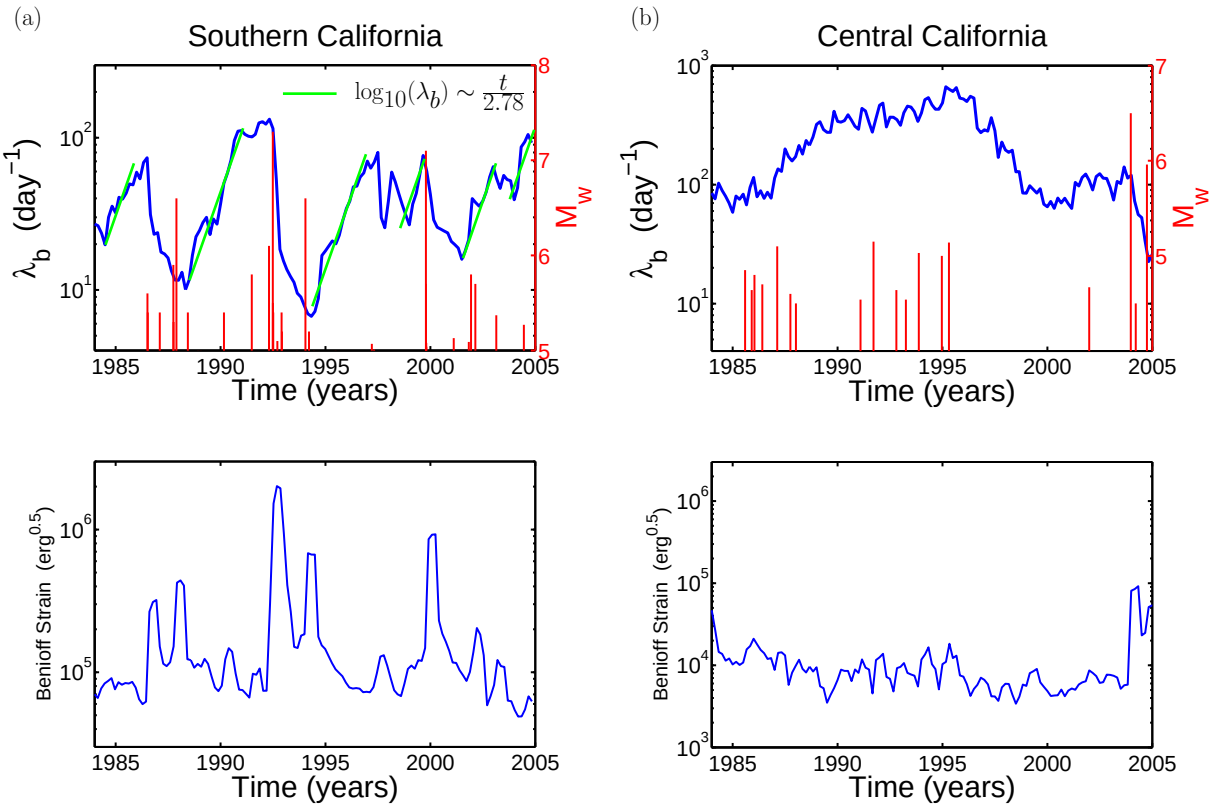

Figure 8. Evolution of the λ_b value (top) and of the Benioff strain accumulated over the moving time window (bottom) in southern California (a) and central California (b). In top figures, secondary axes show $M > 5$ earthquakes in southern California and $M > 4$ earthquakes in central California. For southern California, green lines indicate a constant trend in a logarithmic scale ($\log_{10}(\lambda_b) \sim t/t_0$ with $t_0 \approx 2.78\ yr$).

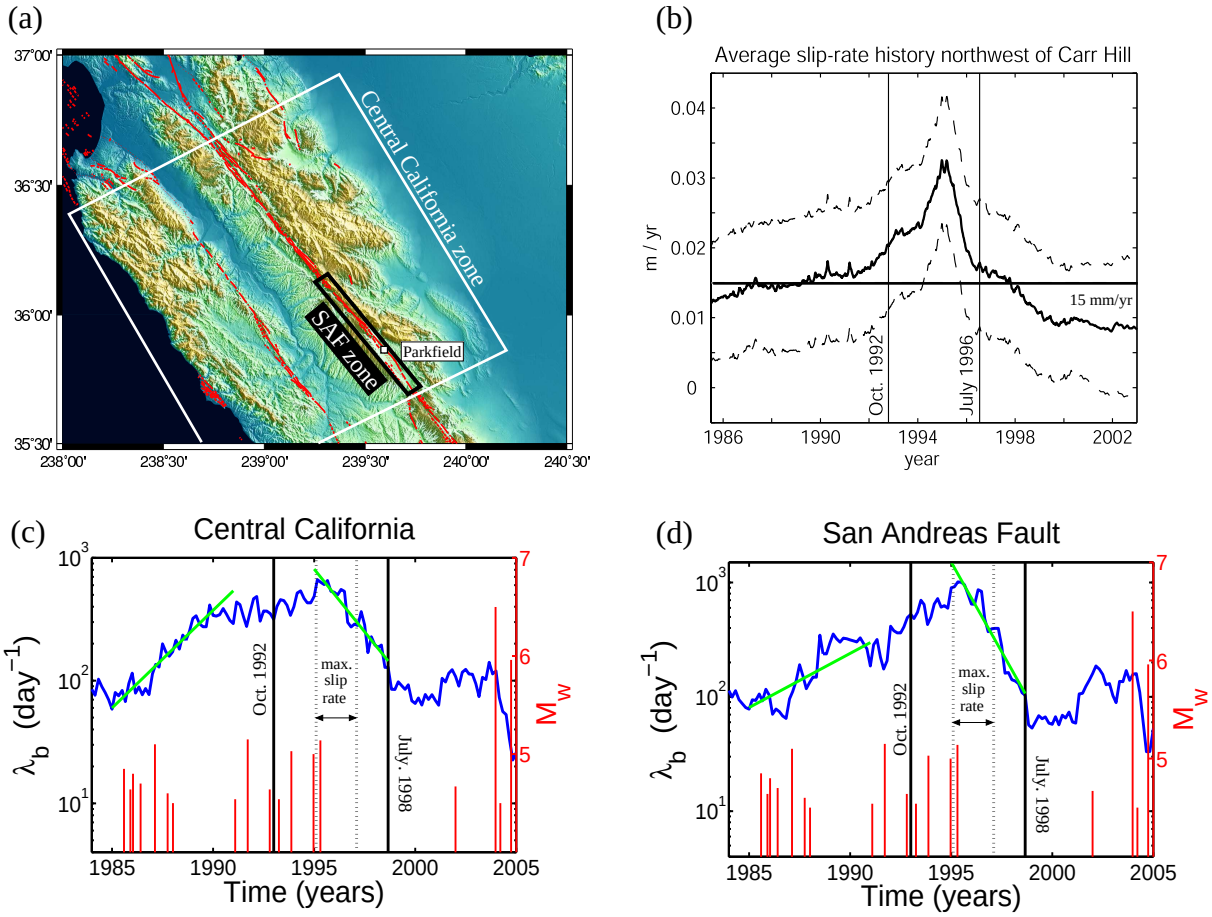

Figure 9. Comparison between (b) the temporal evolution of the average slip-rate on a fault segment northwest of Carr Hill obtained by *Murray and Segall* [2005] and (c) the evolution of the λ_b value in central California and (d) along the SAF near Parkfield (zones are shown in (a)). In (c) and (d), solid lines limit λ_b values calculated from aftershocks that occurred only between October 1992 and July 1998. Dashed lines limit λ_b values calculated over a time period that incorporate the maximum of slip rate. Green lines are regression lines that follow $\log_{10}(\lambda_b) \sim t/t_0$ with $t_0 = 6.67\ yr$ from 1987 to 1990 and $t_0 = -4.76\ yr$ from 1995 to 1998 for (c) and with $t_0 = 11.1\ yr$ from 1987 to 1990 and $t_0 = -3.23\ yr$ from 1995 to 1998 for (d).

Time period	Type	Velocity ($mm.yr^{-1}$)
pre 1991	V_0	10.4 ± 0.5
1991-1993	ΔV_1	-1.5 ± 1.5
1993-1998	ΔV_2	$+3.3 \pm 0.9$

Table 2. Results of the inversion of *Gao et al.* [2000] from the examination of the Parkfield deformation dataset, particularly those from the two color electronic distance meter. V_0 is an apparent velocity estimate and $\Delta V_{1,2} = V_0 - V_{1,2}$ are transient velocities.

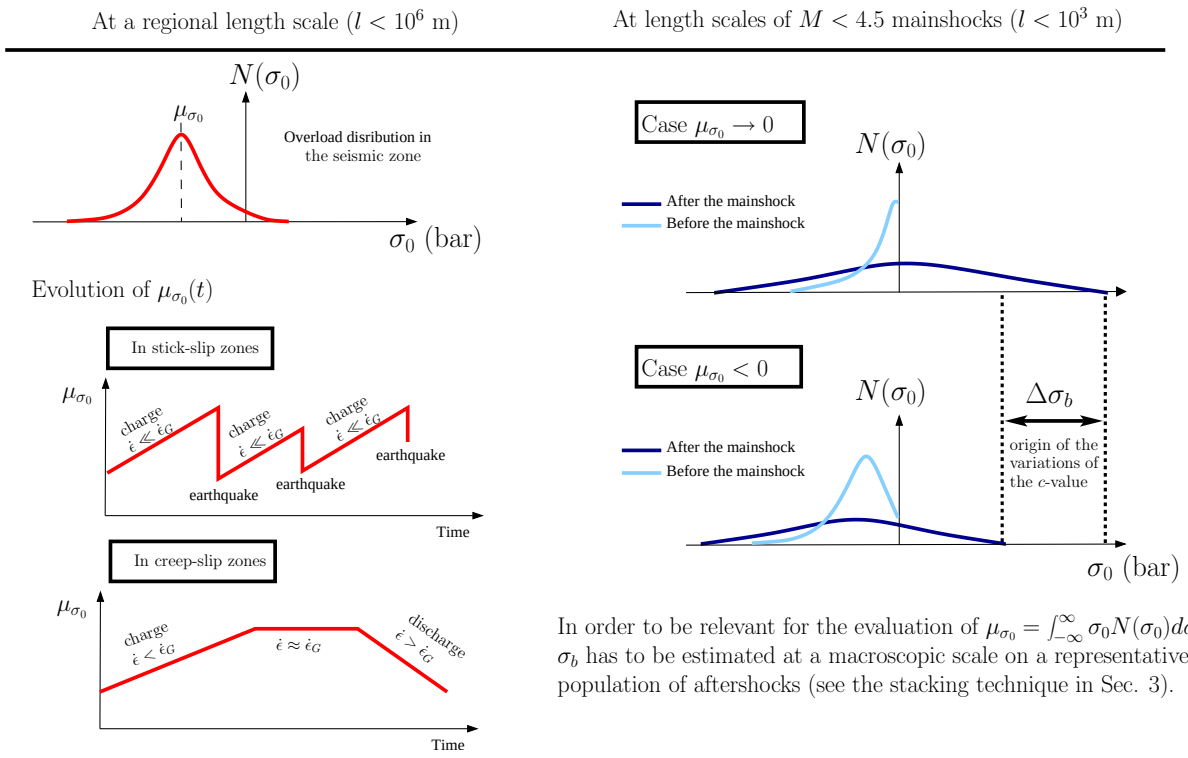

Figure 10. Schematic representation of the relationship between different deformation modes and λ_b (or c) a statistical parameter extracted from catalogs of seismicity. Note that $\dot{\epsilon}$ and $\dot{\epsilon}_G$ are the strain accumulation rate and the long-term geological strain rate respectively. μ_{σ_0} is the mean value of the overload at a given time. The σ_b value is a function of the λ_b value (see Fig. 1). Hence, assuming that σ_b is positively correlated with μ_{σ_0}, the evolution of the λ_b value could be connected to loading/unloading rates in the brittle upper crust, especially where aseismic deformation transients occur.

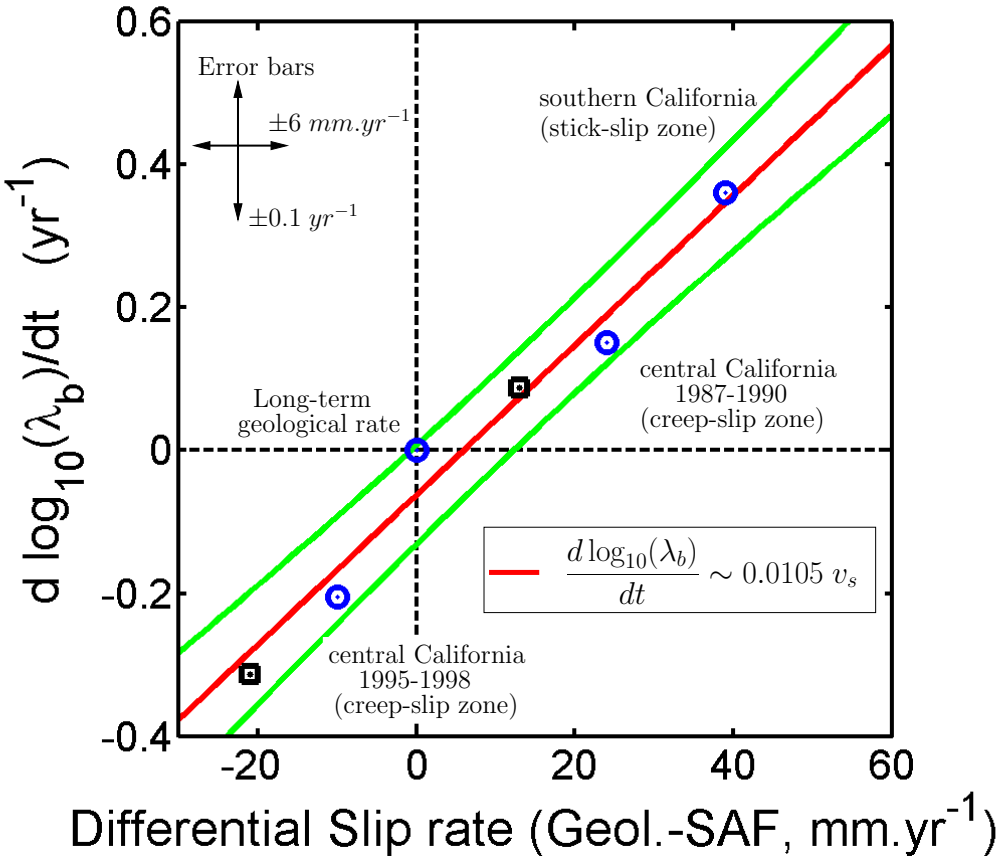

Figure 11. Relationship between $d\log_{10}(\lambda_b)/dt$ and the deficit of slip rate between the long-term geological rate and the slip rate across the SAF. Circle and square symbols corresponds to zones with widths of 200 km and 1 km centered on the SAF (see Figs. 8 and 9). Taking into account the increase of right lateral deformation rate with distance from the fault, we consider geological slip rates of 39 $mm.yr^{-1}$ for circles and 28 $mm.yr^{-1}$ for squares (see text). The red line is the best fit straight line obtained by regression ($r^2 = 0.974$). The green lines demarcate the 95% prediction interval of the regression line.

Region	W (km)	Time period	v_g $(mm.yr^{-1})$	v $(mm.yr^{-1})$	v_s $(mm.yr^{-1})$	$\frac{d \log_{10}(\lambda_b)}{dt}$ (yr^{-1})
central	200	1987-1990	39	15	24	0.15
central	200	1995-1998	39	49	-10	-0.21
southern	200	Inter-seismic	39	0	39	0.36
central	1	1987-1990	28	15	13	0.09
central	1	1995-1998	28	49	-21	-0.31

Table 3. Relationship between the evolution rate of the λ_b value in logarithmic scale and the deficit of slip rate $v_s = v_g - v$. W is the characteristic length scale of the zone under consideration perpendicularly to the SAF plane, v is the maximum slip rate estimated from geodetic measurements [*Murray and Segall*, 2005], and v_g the long term geological slip rate [*Titus et al.*, 2005].

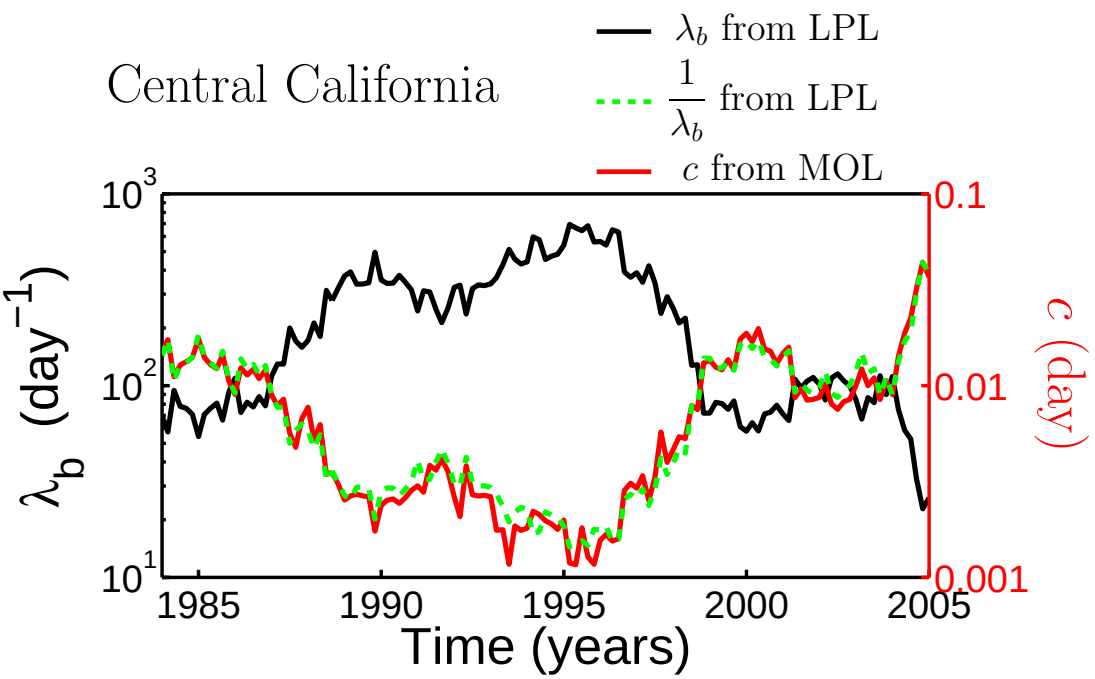

Figure 12. Evolution of λ_b (black), $1/\lambda_b$ (green dotted), and c (red) from 1984 to 2005 in central California. Independent fits of the MOL (c) and the LPL (λ_b) give similar estimations of the time delay before the onset of the power law decay rate.

Figure 13. Evaluation of the stability of the signal shown in Fig. 9 through the parameter space of the aftershock selection procedure. Each figure represents the evolution of λ_b and of the number of aftershocks in the stacks from 1984 to 2005 in the SAF and central California zones (see Fig. 9a). We test (a) different magnitude thresholds for mainshocks and aftershock in order to minimize M_Δ (Eq. 7). (b) different time windows to estimate the impact of time averaging. (c) different parameters for the declustering algorithm of *Gardner and Knopoff* [1974] (Tab. 1). (d) another declustering method for which the space window is scale on the magnitude of the mainshock. Insets indicate parameters that have been changed. Defaults values are $M_M^{Min} = 2.5$, $M_M^{Max} = 4.5$, $M_A^{Min} = 1.8.$, $\Delta T_w = 2\ yrs$, and the L and T values indicated in Tab. 1. The black dotted lines indicated the trends that have been estimated in Fig. 9 for periods of 1987-1990 and 1995-1998.

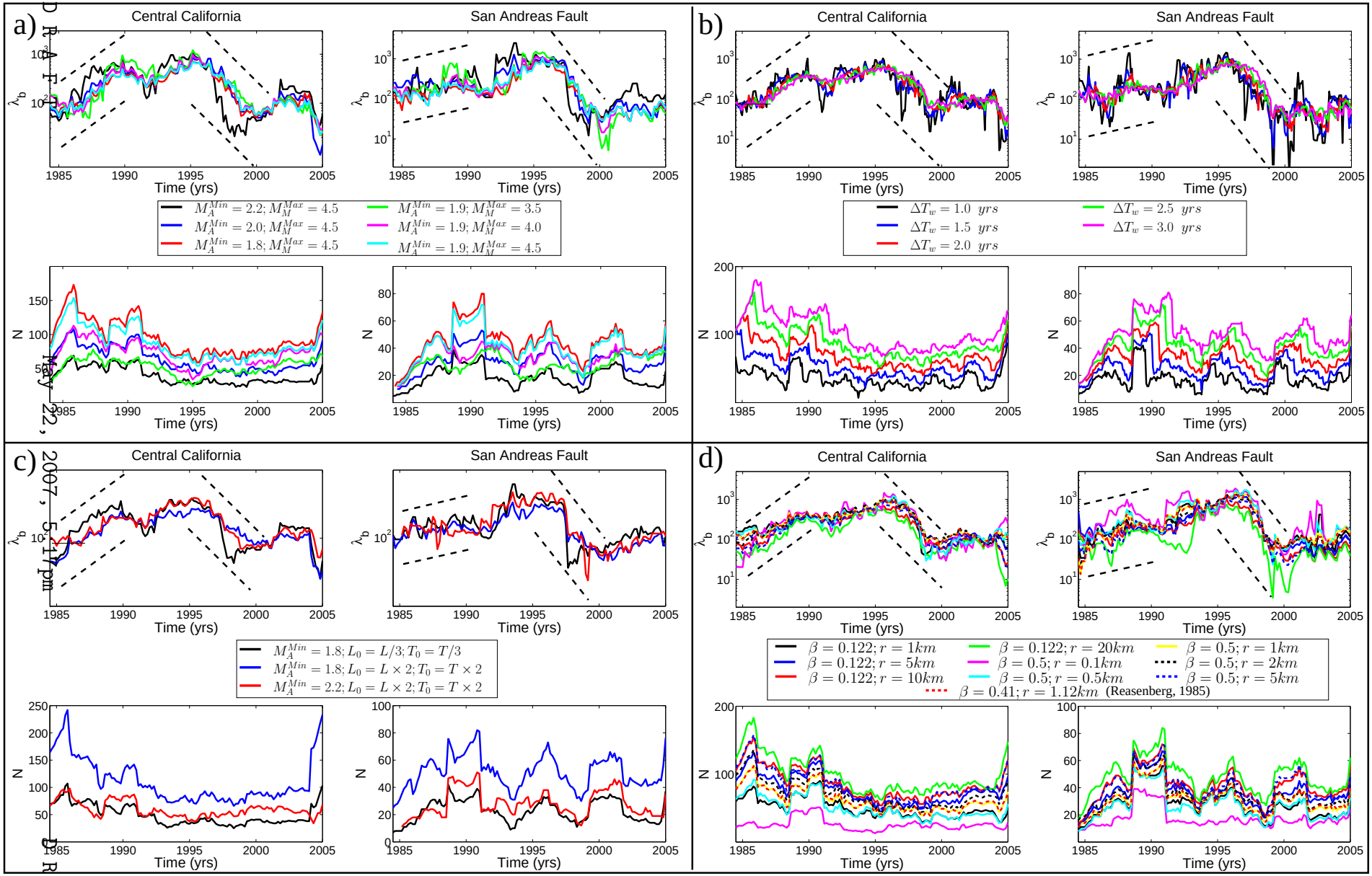

Figure 13.